










Evidence of Environmental Quenching at Redshift $z \approx 2$

Zhiyuan Ji¹ , Mauro Giavalisco¹ , Christina C. Williams² , Sandra M. Faber³, Henry C. Ferguson⁴ , Yicheng Guo^{3,5} ,
Teng Liu^{1,6} , and Bomee Lee^{1,7} 

¹ University of Massachusetts Amherst, 710 North Pleasant Street, Amherst, MA 01003-9305, USA; zhiyuanji@astro.umass.edu

² Steward Observatory, 933 North Cherry Avenue, University of Arizona, Tucson, AZ 85721, USA

³ University of California Observatories/Lick Observatory, University of California, Santa Cruz, CA 95064, USA

⁴ Space Telescope Science Institute, 3700 San Martin Boulevard, Baltimore, MD, 21218, USA

⁵ Department of Physics and Astronomy, University of Missouri, Columbia, MO, 65211, USA

⁶ University of Science and Technology of China, Hefei, Anhui, 230026, People's Republic of China

⁷ Infrared Processing and Analysis Center, California Institute of Technology, Pasadena, CA 91125, USA

Received 2017 June 2; revised 2018 May 2; accepted 2018 June 10; published 2018 July 31

Abstract

We report evidence of environmental quenching among galaxies at redshifts of ≈ 2 , namely the probability that a galaxy quenches its star formation activity is enhanced in the regions of space in proximity of other quenched, more massive galaxies. The effect is observed as strong clustering of quiescent galaxies around quiescent galaxies on angular scales of $\theta \leq 20$ arcsec, corresponding to a proper (comoving) scale of 168 (502) kpc at $z = 2$. The effect is observed only for quiescent galaxies around other quiescent galaxies; the probability to find star-forming galaxies around quiescent or around star-forming ones is consistent with the clustering strength of galaxies of the same mass and at the same redshift, as observed in dedicated studies of galaxy clustering. The effect is mass dependent in the sense that the quenching probability is stronger for galaxies of smaller masses ($M_* < 10^{10} M_\odot$) than for more massive ones, i.e., it follows the opposite trend with mass relative to gravitational galaxy clustering. The spatial scale where the effect is observed suggests that these environments are massive halos, in which case the observed effect would likely be satellite quenching. The effect is also redshift dependent in that the clustering strength of quiescent galaxies around other quiescent galaxies at $\bar{z} = 1.6$ is $\approx 1.7 \times$ larger than that of the galaxies with the same stellar mass at $\bar{z} = 2.6$. This redshift dependence allows for a crude estimate of the timescale of environmental quenching of low-mass galaxies, which is in the range of 1.5 \sim 4 Gyr, in broad agreement with other estimates and with our ideas on satellite quenching.

Key words: cosmology: observations – galaxies: evolution – galaxies: high-redshift

1. Introduction

Observations both in the local universe and at high redshift have clearly shown that galaxies are characterized by a distinct bimodality of star formation and dynamical properties and that is reflected in a corresponding bimodality of colors, morphology types, and specific star formation rates (SSFRs; Baldry et al. 2004, 2006; Wyder et al. 2007; Bamford et al. 2009; Blanton & Moustakas 2009). Particular attention has been devoted to the physics of quenching, which refers to the sets of processes that shut down the star formation activity inside galaxies and drive the transformation of galaxies from one type of the bimodality to the other, i.e., from a star-forming galaxy to a quiescent one. These processes remain observationally unconstrained.

While the detailed physical mechanisms of quenching are unclear, phenomenologically two broad categories of quenching mechanisms have been identified—“mass quenching” and “environmental quenching” (Peng et al. 2010; Schawinski et al. 2014). Mass quenching generically refers to processes internal to a galaxy that depend on (or correlate with) the mass of the galaxy, like AGN and stellar feedback (Fabian 2012; Hopkins et al. 2012), morphological quenching (Martig et al. 2009) or halo mass shock heating (Dekel & Birnboim 2006). For example, the strong correlation between the presence of a massive bulge and the probability the galaxy is quenched (Drory & Fisher 2007) has been interpreted as evidence that the central AGN may affect quenching (Franx et al. 2008; Cheung et al. 2012; Barro et al. 2015). Whitaker

et al. (2017) reported a tight correlation between the central stellar surface density and the star formation activity, namely the fact that as galaxies quench they also develop a central structure characterized by high stellar mass density. This would imply a common mechanism (or mechanisms) controlling both the growth of the central regions of galaxies and the cessation of their global star formation activity.

Unlike mass quenching, environmental quenching is associated with the external environment of a galaxy and it is considered to be an effective quenching mechanism of galaxies in dense environments (e.g., galaxy groups/clusters). A number of specific mechanisms have been proposed for environmental quenching. For example, when a galaxy with a relatively small halo (satellite) is accreted by a massive halo, its gas supply from accretion from the cosmic web can be cut off. This will lead to a gradual quenching in a long timescale as the satellite exhausts its own gas and is usually known as “gas strangulation” (Larson et al. 1980; van den Bosch et al. 2008; Peng et al. 2015). If the external pressure by the surrounding medium, i.e., the inter-cluster medium (ICM) or inter-group medium, is high enough, ram pressure stripping may also be able to remove cold gas from the satellite in a relatively short timescale, resulting in a rapid quenching (Gunn & Gott 1972). Apart from the above two mechanisms, a process called “galaxy harassment” is also proposed for environmental quenching (Farouki & Shapiro 1981; Moore et al. 1998), which refers the interactions between the satellite with high-speed fly-bys. The cumulative effect of many high-speed

encounters can also significantly change the morphology of the satellite.

The correlations between stellar mass, star formation, and environment observed in the local universe (Gómez et al. 2003; Balogh et al. 2004; Hogg et al. 2004; Kauffmann et al. 2004; Blanton et al. 2005) have also been found to persist out to at least $z \sim 1$ (Cucciati et al. 2006; Cooper et al. 2007; Peng et al. 2010; Sobral et al. 2011; Kawinwanichakij et al. 2017; Papovich et al. 2018). If these trends are indicative of both mass quenching and environmental quenching processes operating independently, then these processes must have already been in place by $z \gtrsim 1$. In fact, Guo et al. (2017) find likely evidence of environmental quenching at $0.5 < z < 1$ based on the spatial distribution of low-mass ($8.0 < \text{Log}_{10}(M_*/M_\odot) < 9.5$) quiescent galaxies around massive ($\text{Log}_{10}(M_*/M_\odot) > 10.5$) neighbors. Newman et al. (2014) conduct the study of a rich cluster at $z = 1.8$, where they find the cluster environment is more efficient in suppressing star formation. Also, work by Lin et al. (2012) on the clustering properties of bright BzK-selected galaxies at $z \sim 2$ finds evidence that the strength of galaxies’ spatial clustering depends on their star formation properties, both star formation rate (SFR) and SSFR, which they interpret as evidence that the environment has probably started to play a role in quenching star formation already at that epoch.

Measuring the comparative strength of spatial clustering of galaxies as a function of their star formation activity indeed offers a powerful tool to investigate the phenomenology of quenching in galaxies at high redshift (e.g., $z > 1$) and the correlations between star formation activity and the environment, when large and well characterized samples are available (e.g., Coil et al. 2017). Spectroscopic observations of high-redshift galaxies is resource-intensive, however, and even 8–10 m telescopes can only observe relatively bright galaxies and with a strong bias against quiescent galaxies. In particular, for statistical studies of spatial clustering, we do not have big enough spectroscopic samples of quiescent galaxies at $z > 1$ to perform a robust spatial distribution analysis. Angular clustering, or other diagnostics of the relative angular proximity of galaxies (e.g., Guo et al. 2017), however, provides a robust alternative. In particular, the availability of large and deep multiband photometric surveys from space, CANDELS (Grogin et al. 2011; Koekemoer et al. 2011), and the consequent improvement of photometric redshifts and spectral energy distribution (SED) fitting techniques, means that we can now probe the correlation between environmental effects and star formation activity in the high-redshift universe.

In this work, we study the environmental effects on quenching galaxies at high redshift, where we consider the environment as the volumes immediately around galaxies (e.g., $r < R_{\text{vir}}$). We use H -band selected galaxies in GOODS fields (Giavalisco et al. 2004) from CANDELS. We measure the small-scale angular correlation function for different types of galaxies and investigate possible evidence of environmental effects on star formation activity at redshift $\bar{z} \approx 2$ (mean redshift of our sample). In this paper, we adopt a Λ CDM cosmology with the parameters: $\Omega_m = 0.3$, $\Omega_\Lambda = 0.7$, and $h = H_0/(100 \text{ kms}^{-1} \text{ Mpc}^{-1}) = 0.7$.

2. Method

The goal of this study is to investigate how star formation activity changes with the environment at $\bar{z} \approx 2$ by means of a comparative analysis of the strength of the angular clustering of quiescent and star-forming galaxies. In Section 2.1, we describe the data selection and their division to quiescent and star-forming

samples. In Section 2.2, we present how we measure the angular clustering of the samples.

2.1. The Data and The Samples

Our main sample consists of 9887 galaxies culled from both the regions of the GOODS-S ($\approx 0.05 \text{ deg}^2$) and GOODS-N fields ($\approx 0.05 \text{ deg}^2$) that have been observed with *HST*/WFC3 as part of the deep portion of the CANDELS program (Grogin et al. 2011; Koekemoer et al. 2011). In this work, we have taken advantage of the deep CANDELS multiwavelength photometry available in the GOODS fields and the official CANDELS photometric redshift catalog (see Dahlen et al. 2013; Hsu et al. 2014) in which the full pdf is used in the determination of photometric redshift obtained with the EAZY code (Brammer et al. 2008) and the templates by Muzzin et al. (2013). A number of papers have presented measures of stellar mass in the CANDELS fields (Tomczak et al. 2014; Mobasher et al. 2015; Santini et al. 2015). Here we have used the measures of stellar mass obtained by Lee et al. (2018), which adopts an advanced Markov chain Monte Carlo (MCMC) SED fitting procedure that treats the star formation history (SFH) of the galaxies as a free “parameter” to obtain robust estimates of the stellar mass, SFR, and (luminosity weighted) mean stellar age. These measures of stellar mass are in excellent agreement with the other works (see Figure 5 in Lee et al. 2018). We have selected our sample galaxies to be in the redshift range of $1.2 < z < 4$ using spectroscopic redshift ($\approx 6\%$) whenever available or photometric ones and for having stellar mass $M_* > 10^9 M_\odot$. To secure high-quality photometry, and hence high-quality photo- z and SED fitting stellar mass measures, we have also required the isophotal H -band signal-to-noise ratio to be $S/N > 10$.

To classify our galaxies as quiescent or star-forming, we have used the UVJ-color selection method proposed by Williams et al. (2009), for which we have calculated the region of quiescent galaxies using spectral population synthesis models from Bruzual & Charlot (2003), illustrated in Figure 1. We have also verified that the UVJ-selected samples of quiescent and star-forming galaxies are in excellent agreement with an analogous definition based on direct measures of SSFR, as discussed, for example, in Lee et al. (2018). In what follows, we define galaxies inside the quiescent region of the UVJ diagram as “quiescent” or “quenched” galaxies and those outside as “star-forming” galaxies. The final quiescent sample contains 294 galaxies in the GOODS-S field and 254 galaxies in the GOODS-N field, while the star-forming sample includes 4977 galaxies in GOODS-S and 4362 galaxies in GOODS-N. Figures 2(a) and (b) show the (mostly photometric) redshift and stellar mass distributions for the combined star-forming and quiescent samples. Figure 2(c) shows the angular distributions for the quiescent and star-forming samples in GOODS-S and GOODS-N respectively. Our quiescent samples are not located in one or two clusters, instead, they cover all across the two fields.

We have used the simulations by Guo et al. (2013) in GOODS to estimate the completeness in our sample to be $\approx 80\%$. As shown in Figure 3, the majority of selected galaxies occupies the region where sample completeness is $> 80\%$. A few sources (mostly in the high redshift) are in the region with completeness between 50% and 80%. As we will discuss later, incompleteness does not substantially affect our conclusions because it does not impact measures of angular clustering as

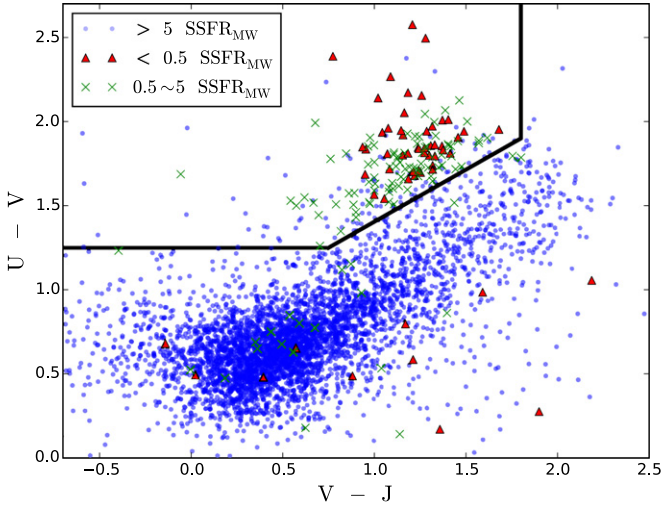


Figure 1. UVJ selection and comparison with SED fitting results. Three colors represent three SSFR bins, where we assume $SSFR_{MW} \sim 2/(8 \times 10^{10}) \text{ yr}^{-1}$. Galaxies in the upper left region defined by the dashed lines are defined as quiescent galaxies in this work.

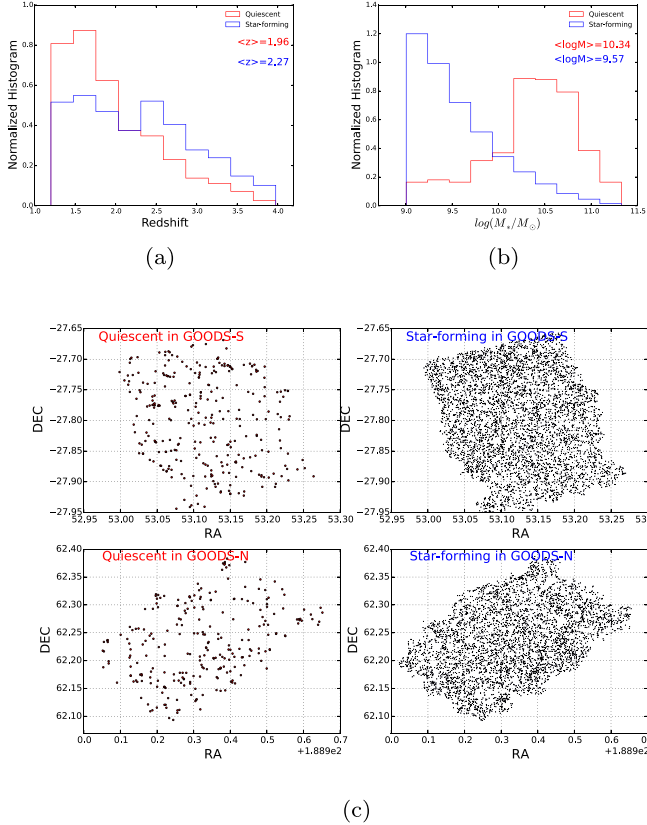


Figure 2. (a) Redshift distributions for quiescent sample with mean redshift $\bar{z} = 1.96$ and star-forming sample with $\bar{z} = 2.27$, (b) best-fit stellar mass (M_*) distributions for quiescent sample with mean stellar mass $\bar{M}_* = 10^{10.34} M_\odot$ and star-forming sample with $\bar{M}_* = 10^{9.57} M_\odot$, and (c) angular distributions on the sky for quiescent and star-forming samples in GOODS-S and GOODS-N.

long as there is no spatial dependence on the probability for a galaxy of making into the samples or not, which we do not observe. We will see that incompleteness only quantitatively affects our measures of the quenched fraction, i.e., the ratio of the number of quiescent galaxies to the total number of

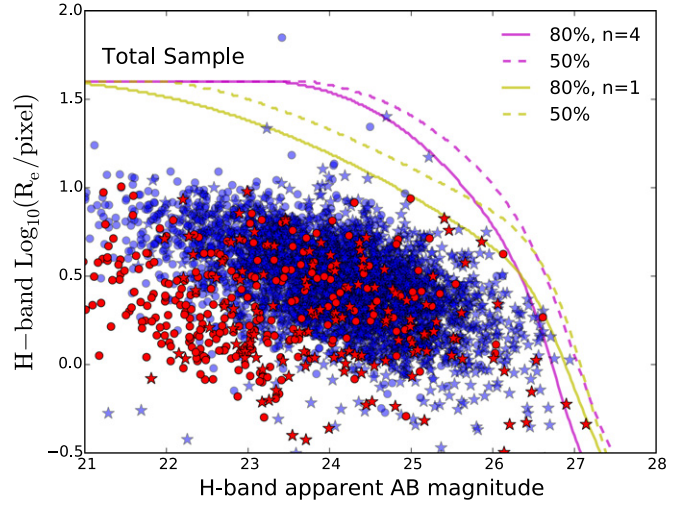


Figure 3. Completeness estimated from the simulations by Guo et al. (2013). The light profile of fake sources is assumed to be an exponential disk (*Sérsic index* $n = 1$, yellow) or a de Vaucouleurs profile ($n = 4$, magenta). In each case, the constant curves of 50% (dashed) and 80% (solid) completeness are plotted. Star-forming (blue) and quiescent (red) galaxies selected in this work are shown. The points and stars are for galaxies at $z < 2$ and $z > 2$ respectively.

galaxies. The magnitude of the effect, however, does not affect our conclusions.

2.2. Angular Clustering Amplitude Measurement

The angular two-point correlation function $\omega(\theta)$ is defined as the excess probability, above that expected for a homogeneous (*Poisson*) distribution, of finding two galaxies with an angular separation θ within a solid angle $\delta\Omega$ (Peebles 1980) projected in the sky. In this work, we use the estimator of angular correlation function proposed by Landy & Szalay (1993):

$$\omega(\theta) = \frac{DD(\theta) - 2DR(\theta) + RR(\theta)}{RR(\theta)}, \quad (1)$$

where $DD(\theta)$ is the number of pairs of observed galaxies with angular separations in the range $(\theta, \theta + \delta\theta)$, $DR(\theta)$ is the number of cross-pairs between the observed galaxies and a randomly distributed sample and $RR(\theta)$ is the number of the randomly distributed pairs.

A random catalog of sources must be produced with the same sky coverage, geometry, and spatially dependent detection incompleteness. We generate the random samples by inserting 3000 randomly positioned sets of fake sources into the noise map of GOODS-S and GOODS-N respectively. The inserted sources have the same H -band magnitude distribution as what is observed for our galaxy sample. We generate 20 of these simulations and select the random sources ($\approx 50,000$ in total) that are retrieved by SExtractor (Bertin & Arnouts 1996) with 10 S/N. We calculate the angular correlation function of these retrieved random sources and have verified that on average the random sources in the simulation are unclustered, i.e., $\omega(\theta) = 0$.

We estimate the random errors on the two-point angular correlation function at each angular bin by two methods—bootstrap resampling and spatial jackknife resampling. For bootstrap, we generate 100 resamplings of the original sample, each containing N galaxies (including duplicates) randomly picked from the original N galaxies with replacement, i.e., a

Table 1

Random Errors Estimated by Bootstrap Resampling and Spatial Jackknife Resampling for the Quiescent Sample on Small Angular Scales

$\text{Log}_{10}(\theta/\text{arcsec})$	$\sigma_{\text{bootstrap}}$	$\sigma_{\text{jackknife}}$
0.2	3.57	3.14
0.4	1.74	2.30
0.6	0.96	0.88
0.8	0.51	0.44
1.0	0.32	0.24

galaxy is retained in the stack even if it has already been picked. Then we estimated the error bar of bootstrap resampling by:

$$\sigma_{\text{bootstrap}}^2 = \frac{1}{N_{\text{rs}}} \sum_k^{N_{\text{rs}}} (\omega_k(\theta) - \bar{\omega}(\theta))^2, \quad (2)$$

where $N_{\text{rs}} = 100$, $\omega_k(\theta)$ denotes the measurement of $\omega(\theta)$ from the k th resampling and $\bar{\omega}(\theta)$ is the mean obtained from the 100 bootstrap resampling. For the spatial jackknife sampling, we quantify the error bars by binning GOODS-S and GOODS-N fields into 25 nonoverlapping areas, respectively, and calculate the jackknife errors by

$$\sigma_{\text{jackknife}}^2 = \frac{N-1}{N} \sum_{k=1}^N (\omega_k(\theta) - \bar{\omega}(\theta))^2, \quad (3)$$

where $N = 25$ areas, $\omega_k(\theta)$ is calculated with the k th area removed, and $\bar{\omega}(\theta)$ is the average values of $\omega_k(\theta)$. As listed in Table 1, random errors on small angular scales (<10 arcsec) estimated by these two methods are comparable. The jackknife errors, in general, are slightly smaller than those estimated by bootstrap resampling, so we conservatively adopt the bootstrap errors in this work. Estimating systematic errors of $\omega(\theta)$ is more involved, since this needs to take into account the geometry and size of the observed field to model the strength of the integral constraints (IC) bias. As will become clear later, our goal in this study is a comparison of the relative strength of the angular clustering of various subsamples of galaxies extracted from the same main sample rather than the measure and fitting of the correlation function in each case. Since, to a large extent, each measure of $\omega(\theta)$ is subject to the same IC bias, we have not included the correction because it will not affect the sense of the comparison of the relative strength of the clustering signal in our subsamples.

Figures 4 and 5 show the measured $1 + \omega(\theta)$ for the main subsamples, namely the auto-correlation function of quiescent galaxies, the auto-correlation function of star-forming galaxies, and the cross-correlation function of star-forming galaxies and quiescent galaxies. The figures (also Table 2) illustrate the main result of this study: the auto-correlation function of quiescent galaxies is much larger than that of star-forming galaxies, while the auto-correction of star-forming galaxies has the same strength as the cross-correlation of star-forming galaxies and quiescent galaxies. Because the redshift distribution functions of all samples is similar (see Figure 2), differences in the angular clustering directly translates into similar differences in spatial clustering via the Limber transform (see Peebles 1980). In Figure 4, for comparison, we also show the power-law fitted angular correlation functions (already corrected for the IC)

collected from the literature for other high-redshift samples— Lyman Break Galaxies (LBGs) at redshift 3 from Giavalisco et al. (1998) (G98), BzK color-selected galaxies at redshift 2 from Kong et al. (2006, hereafter K06), and Hayashi et al. (2007, hereafter H07).

The auto-correlation function of our sample of star-forming galaxies is quantitatively comparable to that of the low-mass sample of star-forming BzK galaxies from H07, which cover the same redshift range, and it is also similar to that of LBG at $z \sim 3$ (G98). Both types of star-forming galaxies are similar to ours and should be hosted in dark-matter halos covering a similar mass range. The figure also shows the measured auto-correlation function of dark-matter halos expected to host the high-mass star-forming BzK (K06) galaxies. An excess at small angular scales that is of similar magnitude to that of the quiescent auto-correlation function is not observed in any case.

Note that neglecting the IC correction is not likely to significantly affect the comparison of the relative clustering strength of the subsample we have considered. First and foremost, the IC correction relates to the large-scale behavior of the correlation function, where the effect of the finiteness of the samples are affected by the lack of knowledge of the number density of the parent population, while the small-scale clustering considered here is dominated by the structure of the halos. Secondly, when measured over sufficiently large volumes, the Landy & Szalay (1993) estimator of the angular correlation function that we have used here underestimates the true clustering due to the IC bias (Hamilton 1993). This bias depends itself on the strength of the clustering of the galaxies being considered, and it is larger for more clustered galaxies (see Adelberger et al. 2005; their Equation (13)). Since we average together GOODS-N and GOODS-S fields and both the transverse and radial size of each field is much larger than the galaxy correlation length, neglecting the IC correction for the most strongly clustered sample results in underestimating its true strength more than it does for the more weakly clustered sample, which reinforces our conclusions.

Incompleteness, which affects our sample mostly in the high-redshift bin at the low end of the stellar mass distribution, does not significantly affect the results or our conclusions, unless it is a function of the environment such that the incompleteness is higher in the field and lower in the dense environment, an occurrence for which there is no evidence. In fact, one would expect the opposite effect to happen because the background level and isophote confusion in a denser environment are higher than in the field, which would make the detection probability of galaxies in denser environments more incomplete than in the field.

3. Discussions

3.1. Evidence of Environmental Quenching

As shown in Figure 4 and listed as $\omega_{\text{Q}}/\omega_{\text{SF}}$ in Table 2, the auto-correlation functions of quiescent and star-forming galaxies are similar at large scales ($\gtrsim 30$ arcsec, corresponding to $\gtrsim 1$ Mpc comoving scale). The excess clustering strength of the quiescent sample is mainly observed within $\lesssim 20$ arcsec. If we assume an average redshift $\bar{z} = 2$ for the quiescent sample, this angular scale corresponds to a spatial proper (comoving) scale of $r_{\text{q}} \sim 168$ (502) kpc. The small spatial scale seems to suggest that the clustering signal originates inside massive halos, presumably the progenitors of large clusters, in which ram pressure stripping or gas strangulation should be expected

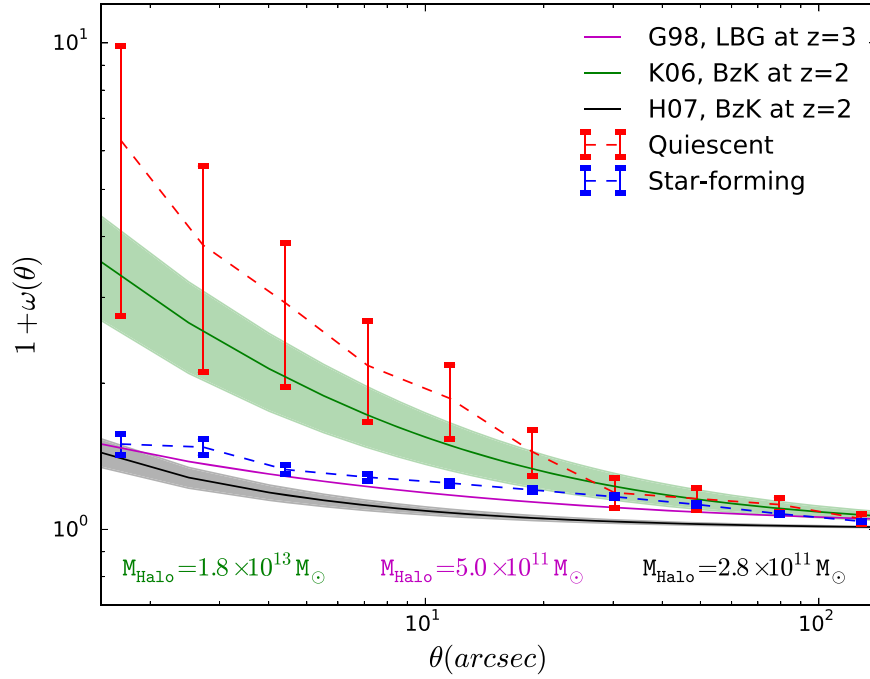


Figure 4. Results of $1 + \omega(\theta)$ for auto-correlation of quiescent galaxies (red) and star-forming galaxies (blue). Three power-law fitted angular correlation functions collected from the literature for other samples are also shown. The magenta solid line with $\omega(\theta) \sim 0.6 \cdot \theta^{-0.5}$ is for LBGs in G98. The best-fit power law is obtained by Porciani & Giavalisco (2002) and halo mass of G98 is estimated as $M_{\text{halo}} = 5 \times 10^{11} M_{\odot}$. The green solid line with $\omega(\theta) \sim 3.46 \cdot \theta^{-0.8}$ (obtained by H07, see their Table 2) is for the subsample (sBzK with $K_{\text{lim}} = 21.9$ mag) of BzK-selected star-forming galaxies in K06. The halo mass of this subsample is estimated by H07 as $M_{\text{halo}} = 1.8 \times 10^{13} M_{\odot}$. The black solid line with a fitted power law of $\omega(\theta) \sim 0.58 \cdot \theta^{-0.8}$ is for H07 BzK-selected galaxies and its halo mass is estimated as $M_{\text{halo}} = 2.8 \times 10^{11} M_{\odot}$. Green and black shaded regions indicate the uncertainty of the best-fit power law for K06 and H07.

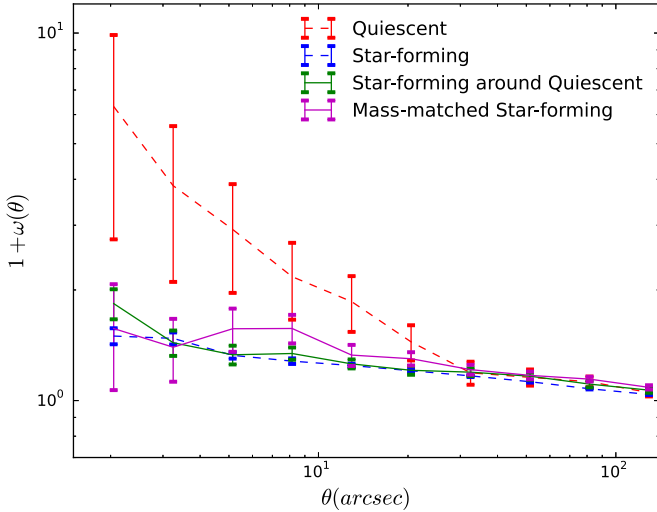


Figure 5. Results of $1 + \omega(\theta)$ for samples of star-forming galaxies that are mass-matched to the quiescent sample (magenta) and star-forming galaxies around quiescent galaxies (green). For comparison, the results for the quiescent sample and star-forming sample are also shown in the plot.

to remove cold gas from infalling low-mass galaxies and terminate their star formation activity. However, since it is not possible for us to distinguish between low-mass galaxies that are satellites residing in massive halos or low-mass galaxies that are centrals of low-mass halos, the observed small-scale clustering actually depends on the relative proportions of satellites and centrals of the same mass. The observed excess clustering of quiescent galaxies therefore could be due to either the mass dependence of halo bias, increased satellite fraction of

quiescent around other quiescent (caused by environmental effects), or both.

Qualitatively, on the same angular scales, because the function $\omega(\theta)$ that we have measured is much larger than that of the much more massive BzK star-forming galaxies at the same redshift selected by K06 (compare the stellar mass distribution of our quiescent samples with Figure 11(f) in K06), the large clustering strength that we observe at small angular scales for the auto-correlation function of quiescent galaxies is unlikely to result from the hosting halo’s bias, which is an increasing function of halo mass and regulates the clustering strength of the general galaxy population. The fact that the two auto-correlation functions at large scales ($\gtrsim 1$ Mpc comoving scale) are similar also indicates the similar “two-halo” term of quiescent and star-forming galaxies. Moreover, we measure the angular cross-correlation function of star-forming galaxies and quiescent galaxies (green solid line in Figure 5). This cross-correlation is, within the errors, the same as the auto-correlation function of star-forming galaxies, indicating that the halo structures of quiescent and star-forming ones are essentially the same. Thus, we interpret the observations as the effects of environmental quenching on clustering, namely of the fact that within massive halos galaxies preferentially quench around other quiescent, more massive galaxies.

The stellar mass distributions of our quiescent sample and star-forming sample are different (Figure 2(b)), with the former being more massive than the latter. Coil et al. (2017) observed that at $z \approx 1.7$ the clustering strength is a significantly stronger function of SSFR than of the stellar mass, suggesting that the difference in stellar mass could only play a minor role in the observed difference of clustering strength. We further investigated whether stellar mass differences between our quiescent and star-forming samples could account for the excess of

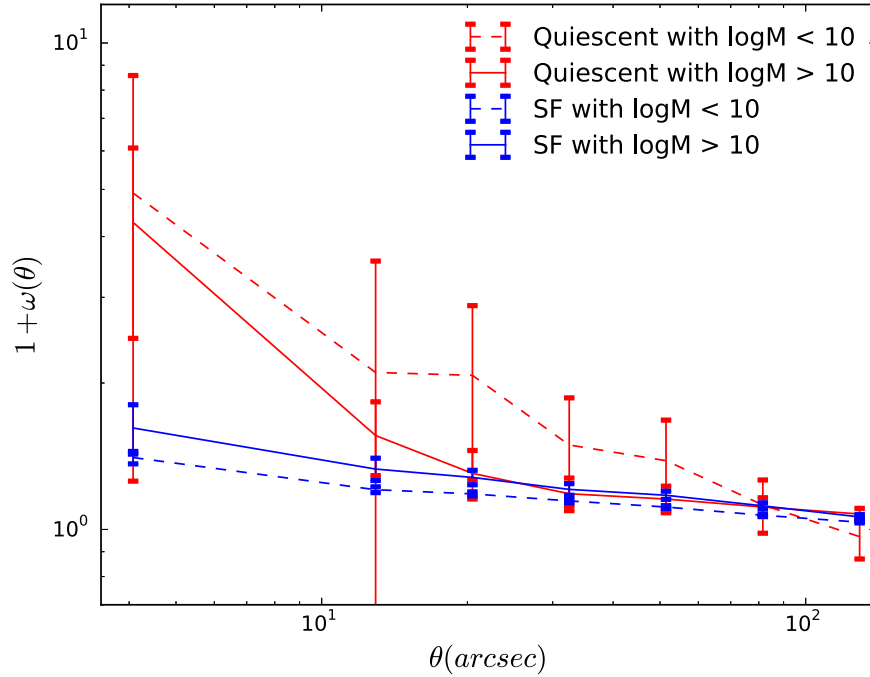


Figure 6. Results of $1 + \omega(\theta)$ for star-forming galaxies (blue) and quiescent galaxies (red) with stellar mass $M_* > 10^{10}M_\odot$ and $M_* < 10^{10}M_\odot$. The low-mass quiescent galaxies show stronger angular clustering than high-mass quiescent galaxies. The low-mass star-forming galaxies show weaker angular clustering than high-mass star-forming galaxies.

Table 2
Angular Correlation Functions in This Work

θ/arcsec	^a D/kpc	^b ω_Q	^b ω_{SF}	^b ω_{cross}	^c $\omega_Q/\omega_{\text{SF}}$	^d $\omega_{\text{cross}}/\omega_{\text{SF}}$
2.0	51.4	5.31 ± 3.57	0.50 ± 0.075	0.84 ± 0.17	10.66 ± 7.34	1.68 ± 0.43
3.2	81.5	2.84 ± 1.74	0.48 ± 0.056	0.44 ± 0.11	5.96 ± 3.72	0.92 ± 0.26
5.1	129.2	1.92 ± 0.96	0.33 ± 0.027	0.33 ± 0.08	5.87 ± 2.97	1.01 ± 0.25
8.2	204.8	1.17 ± 0.51	0.28 ± 0.022	0.34 ± 0.05	4.19 ± 1.86	1.22 ± 0.21
12.9	324.6	0.86 ± 0.32	0.25 ± 0.015	0.26 ± 0.04	3.50 ± 1.33	1.05 ± 0.16
20.5	514.4	0.44 ± 0.16	0.21 ± 0.011	0.21 ± 0.03	2.16 ± 0.78	1.02 ± 0.17
32.5	815.3	0.19 ± 0.09	0.17 ± 0.009	0.19 ± 0.03	1.14 ± 0.52	1.16 ± 0.18
51.5	1292.1	0.16 ± 0.06	0.13 ± 0.006	0.17 ± 0.03	1.25 ± 0.47	1.32 ± 0.21
81.5	2047.9	0.13 ± 0.04	0.08 ± 0.005	0.11 ± 0.02	1.63 ± 0.49	1.41 ± 0.30
129.2	3245.7	0.05 ± 0.03	0.04 ± 0.004	0.07 ± 0.02	1.32 ± 0.66	1.72 ± 0.48

Notes.

^a Comoving scales at $z = 2$.

^b Errors are estimated by bootstrap resampling.

^c Ratio of auto-correlation of quiescent galaxies to that of star-forming galaxies.

^d Ratio of cross-correlation of star-forming and quiescent galaxies to auto-correlation of star formation galaxies.

angular clustering of the quiescent galaxies in the following way. We measure the angular auto-correlation function of mass-matched subsamples of star-forming galaxies whose stellar mass distributions are the same as that of the quiescent sample (magenta solid line in Figure 5). Compared with angular auto-correlation function of star-forming galaxies, the angular clustering increases slightly but the excess is still small compared with auto-correlation of quiescent galaxies. The enhanced clustering signal is consistent with the expected increase due to the larger typical host halo mass of the mass-matched star-forming sample. This investigation indicates that the excess clustering that we observe in the auto-correlation of quiescent galaxies cannot be explained by the higher stellar mass of the sample alone.

As an additional test, we have divided our star-forming and quiescent samples into two stellar mass bins, i.e., $M_* > 10^{10}M_\odot$ and $M_* < 10^{10}M_\odot$. We cannot distinguish central and satellite galaxies in our sample. But, statistically, galaxies in low-mass bin should include larger numbers of satellites (see, e.g., Mandelbaum et al. 2006). Figure 6 shows the angular clustering of star-forming and quiescent galaxies in the two stellar mass bins. The low-mass star-forming galaxies have weaker clustering strength compared with high-mass star-forming ones, which is expected from normal gravitational clustering (i.e., the bias is an increasing function of the dark halo stellar mass), for which more massive galaxies have larger spatial clustering. But the figure shows that the clustering strength of quiescent galaxies in the two stellar mass bins follows

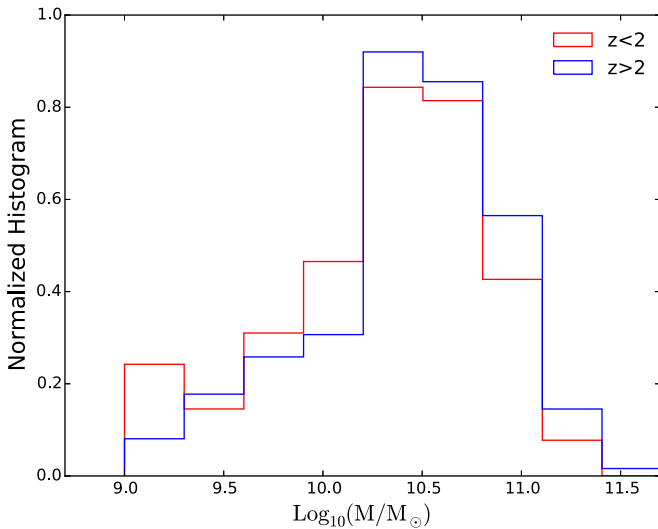


Figure 7. Normalized stellar mass distribution for the low-redshift (red) and high-redshift (blue) quiescent samples.

the opposite trend with stellar mass, with the lower mass bin having the larger clustering strength by a factor of ≈ 1.5 .

We tested the significance of this difference using Monte Carlo simulations, in which we took into account the fact that the individual points of the $\omega(\theta)$ function are not statistically independent but correlated with the following procedure. The simulations test the null hypothesis that the two observed correlation functions are actually two realizations of the same parent population, i.e., both the high- and low-mass samples have the same angular clustering. We first run the simulations by treating each point of $\omega(\theta)$ as independent and then we correct the results to account for the effect of correlation between the points, which we estimate separately. At each angular bin within 100 arcsec, we generate two sets of simulated observations of $\omega(\theta)$, one for the high stellar mass sample and one for the low-mass one, from two Gaussian distributions with the same mean, assumed to be equal to the observations of the high-mass $\omega(\theta)$, and with variance equal to the error bar of each point. In this way, we automatically take into account that the high-mass sample data points have smaller uncertainty than the low-mass ones. We then calculated the probability that the $\omega(\theta)$ of the low-stellar mass sample is found to be smaller by the observed amount at each angular separation point simultaneously. In 10^8 realizations, we found this probability to be 6.25×10^{-4} or $\approx 3.5\sigma$ in a Gaussian statistic. To include the effects of the correlation between the points of $\omega(\theta)$, which results in overestimating the significance of the observed clustering difference of the two mass bins, we used the Monte Carlo simulations by Giavalisco & Dickinson (2001), in which a large number of realizations of galaxy samples is generated with specified intrinsic angular clustering. The measure of $\omega(\theta)$ of each of these samples, therefore, automatically includes the correlation between the points. By repeating the same “null hypothesis” test, in one case using the full “correlated” simulated data set and in another case using two appropriate averaged $\omega(\theta)$ functions (one for the high stellar mass bin and one for the lower one) as “measures” and treating its data points as independent, we derived the correction function to be ≈ 2 . We therefore conclude that the significance of the difference between the angular clustering of the high-mass and low-mass bins is $\approx 1.8\sigma$. The fact that the strength of small-scale clustering for the quiescent

population is smaller in the more massive sample provides further evidence that stellar mass is not the primary parameter that controls the clustering strength in this case, and thus cannot be the reason of the much enhanced clustering of quiescent galaxies compared to every other case. This also indicates that additional factors, e.g., environments, are required to explain the clustering excess that is observed in Figure 4.

3.2. Redshift Dependence of Environmental Quenching

Kawinwanichakij et al. (2016) measured the evolution of the quiescent fraction and quenching efficiency of satellites. For their sample, the satellite quenching is significant at $0.6 < z < 1.6$, while it is only weakly significant at lower or higher redshifts. Hatfield & Jarvis (2017) analyzed a cross-correlation signal for their sample and conclude that at $z \sim 2$ environment is not a significant factor in determining quenching of star-forming galaxies. To understand the redshift dependence of environmental effects, it is crucial to constrain the timescale of environmental quenching from observations. Direct measurements of the timescale of environmental quenching, especially at high redshift, however, remain uncertain because they would require tracking or constraining the infall history of satellite galaxies, which is model dependent. According to recent studies, the quenching time for satellite galaxies is 4.4 ± 0.4 Gyr at $z \sim 0.05$ (Wetzel et al. 2013, based on data from the Sloan Digital Sky Survey (SDSS)); 1.05 ± 0.25 Gyr at $z \sim 0.9$ (Mok et al. 2014, who used the Group Environment Evolution Collaboration 2 (GEEC2)); 1.0 ± 0.25 Gyr at $z \sim 1$ (Muzzin et al. 2014, based on the Gemini CLuster Astrophysics Spectroscopic Survey (GCLASS)); and $2 \sim 5$ Gyr at $z \sim 1-2$ (Fossati et al. 2017, 3D-HST). McGee et al. (2014) argued that the evolution of the satellite quenching timescale could be caused by “orbit-based” (e.g., ram pressure stripping) or “outflow-based” mechanisms and the efficiency of these mechanisms could be different at high redshift. Therefore, estimating the timescale of environmental quenching is critical to constraining the mechanisms at play.

To provide constraints to the timescale of environmental quenching, we have studied how the small-scale clustering of quenched galaxies has evolved with redshift. In particular, we have divided the quiescent sample into two redshift bins, one at $z < 2$ (with mean redshift $\bar{z} = 1.6$) and the other at $z > 2$ (with mean redshift $\bar{z} = 2.6$), and measured the angular clustering of both. As Figure 7 illustrates, these two samples have essentially identical stellar mass distribution. If the redshift evolution of clustering were driven by the growth of structure, as is the case for the general mix of galaxies, the higher redshift sample should be more clustered because of more biased relative to the average mass density distribution (e.g., see Adelberger et al. 2005; Lee et al. 2006, 2009; Tinker et al. 2010). As shown in Figure 8, however, the clustering strength of quiescent galaxies around other quiescent galaxies at $\bar{z} = 1.6$ is $\approx 1.7\times$ larger than that of the same galaxies with the same stellar mass ($M_* \approx 10^{10.35} M_\odot$) at $\bar{z} = 2.6$, which is consistent with Kawinwanichakij et al. (2016) and Hatfield & Jarvis (2017). This is due to the appearance of low-mass quiescent galaxies, whose building-up in the redshift ranges between $z \approx 2.6$ and $z \approx 1.6$ is illustrated in Figure 9. These low-mass galaxies are responsible for the observed strong small-scale angular clustering of quiescent galaxies, which is evidence of environmental quenching taking place around $z \approx 2$. Thus, a

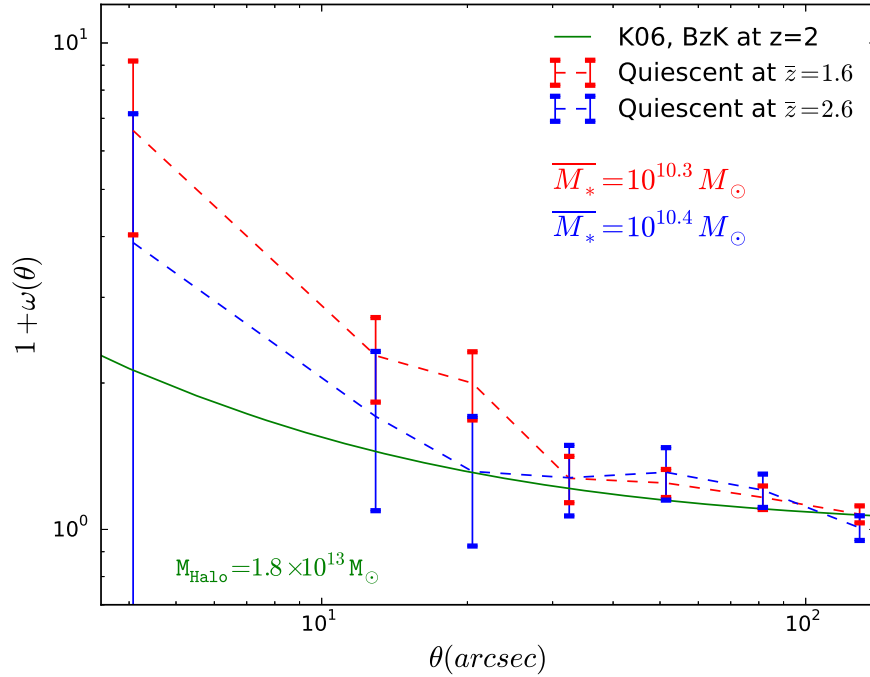


Figure 8. Results of $1 + \omega(\theta)$ for total quiescent galaxies at $z > 2$ (blue) and $z < 2$ (red). The measured $1 + \omega(\theta)$ for BzK galaxies with $M_{\text{halo}} = 1.8 \times 10^{13} M_{\odot}$ from K06 is also shown in the plot. The angular clustering for quiescent galaxies at $z < 2$ is much stronger than BzK galaxies in K06, while statistics for our quiescent galaxies at $z > 2$ are not good enough for comparison.

crude upper limit to the timescale of environmental quenching comes from the age of the universe at the mean redshift, $\bar{z} = 1.6$, of our low-redshift quiescent sample, i.e., ~ 4 Gyr. Another approximate estimate of the timescale over which significant environmental quenching of low-mass galaxies takes place comes from the difference of cosmic time between the average redshift, $\bar{z} = 1.6$ and $\bar{z} = 2.6$, of the two subsamples provides, which is ≈ 1.5 Gyr, consistent with estimates from other groups, as reported earlier.

3.3. Quenched Fraction

More insight into our angular clustering analysis can be gained from looking at the quenched fraction, i.e., the fraction of quiescent galaxies as a function of stellar mass and redshift, which is shown in Figure 9. Although our samples are quite complete (Figure 3), the effect of the relative incompleteness of star-forming and quiescent galaxies must be tested first because if the fractions of missed star-forming and quiescent galaxies differ this causes a systematic error in the shape of the quenched fraction. To check the effects of incompleteness, in particular, to simulate the effects of missing fainter galaxies, we have measured the quenched fraction for the whole sample and also for two additional subsamples obtained by selecting only galaxies that occupy the regions (with sample completeness $> 80\%$) under the solid magenta and yellow curves defined in Figure 3. The quenched fraction for the full sample and for the two subsamples are almost identical. The relative incompleteness therefore will not affect the measured quenched fraction much for our samples.

As Figure 9 shows, the quenched fraction monotonically increases with stellar mass at a fixed redshift, which is interpreted as the primary evidence that there is a key quenching mechanism that correlates with the stellar mass, namely mass quenching (Peng et al. 2010; Birrer et al. 2014).

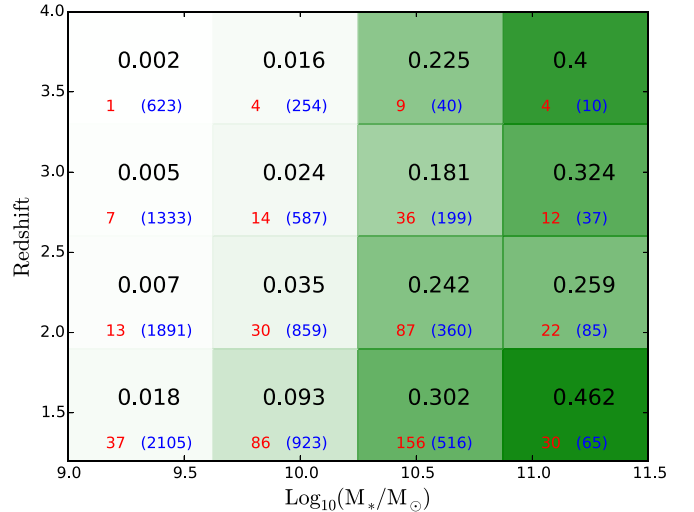


Figure 9. Quenched fraction as a function of stellar mass and redshift. In each bin, the number in black is the quenched fraction, the number in red is the number of quiescent galaxies, and the number in blue is the total number of galaxies.

For a fixed stellar mass, there is weak evidence that the quenched fraction of high-mass galaxies ($\text{Log}_{10}(M_*/M_{\odot}) \gtrsim 10$) evolves with redshift. This is not the case for low-mass galaxies ($\text{Log}_{10}(M_*/M_{\odot}) \lesssim 10$), however, whose quenched fraction shows clear redshift dependence in the sense that the quenched fraction increases as the redshift decreases. This is evidence that some other mechanism, which is not mass quenching and is significantly effective in quenching low-mass galaxies but does not seem to effect high-mass ones, comes into play as the universe evolves.

Recall what has been extensively discussed in previous sections, the excess clustering of quiescent galaxies on small

scales indicates that there is a quenching mechanism dependent on proximity to other quiescent galaxies (i.e., environment). This environmental mechanism seems to be more profound in low-mass galaxies revealed as the inverse stellar mass dependence on auto-correlation of quiescent galaxies. Therefore, the increasing quenched fraction at low-redshift bins is consistent with and very likely to be the result of environmental quenching.

4. Conclusions and Summary

The key observational result of this study is that the angular auto-correlation function of quiescent galaxies on angular scales $\theta \leq 20$ arcsec, which corresponds to a spatial proper (comoving) scale ≈ 168 (502) kpc at $\bar{z} = 2$ (the mean redshift of our sample), is much stronger than that of the general population of galaxies of the same stellar mass, i.e., selected regardless of the specific SFR. It is also much stronger than that of galaxies hosting dark-matter halos an order of magnitude more massive. In other words, at redshift $z \approx 2$ quiescent galaxies cluster around other quiescent galaxies much more strongly than the general galaxy population of the same stellar mass at the same redshift and even $\approx 2\times$ more than galaxies hosting more massive halos. Our measures are in qualitative agreement with the measures of the spatial transverse correlation function by Coil et al. (2017) in the sense that the clustering strength strongly depends on star formation activity of the samples, with galaxies of smaller SFR having stronger clustering strength.

While the strength of galaxy clustering generally increases with the stellar mass of galaxies because more massive galaxies are hosted in more massive dark-matter halos and the bias of the halos is an increasing function of their mass, the opposite is seen for the quiescent galaxies in our sample, i.e., at small angular scales ($\theta \leq 20$ arcsec) the clustering strength of auto-correlation of quiescent galaxies is stronger for lower mass ones. This inverse dependence on the stellar mass implies that the mechanism that increases the bias of quiescent galaxies at small scales must be related with the way these galaxies have quenched their star formation. The spatial scale of the observed excess clustering of the quiescent galaxies suggests that the environment of these galaxies are very massive halos, in which specific mechanisms, such as ram pressure, tidal stripping, or other causes of gas starvation and strangulation (our studies places no constraints on the specifics of such mechanisms) have shut down their star formation activity. We therefore interpret these as evidence of the manifestation of environmental quenching. We also measure the quenched fraction as a function of stellar mass and redshift, which provides evidence of the building-up of low-mass quiescent galaxies, in agreement with our conclusion that some mechanism that is effective at quenching low-mass galaxies comes into play as the universe evolves and is consistent with our interpretation of environmental quenching.








The clustering strength of quiescent galaxies also varies with redshift in the sense that galaxies at $z < 2$ have higher clustering strength than those at $z > 2$. This is also consistent with environmental quenching because we expect the environmental quenching to become more efficient as structures grow (notice that at fixed stellar mass, the clustering of the general population generally increases with increasing redshift because the galaxies are hosted in more massive halos). As we have discussed, this redshift dependence also enables us to put a

crude estimate of the timescale of environmental quenching of low-mass galaxies, $\approx 1.5 \sim 4$ Gyr, which is consistent with results from other studies.

Finally, our results are also in agreement with the similar study by Guo et al. (2017), who use a slightly different statistical description of the angular separation of dwarf quiescent galaxies from the nearest massive ($M_* > 10^{10.5} M_\odot$) galaxy to reach essentially the same conclusions that this provides evidence of environmental quenching at $z \approx 2$.

We thank the anonymous referee for useful comments. The authors acknowledge that the support for HST Programs GO-12060 and GO-12099 was provided by NASA through grants from the Space Telescope Science Institute, which is operated by the Association of Universities for Research in Astronomy, Inc., under NASA contract NAS5-26555.

ORCID iDs

Zhiyuan Ji  <https://orcid.org/0000-0001-7673-2257>
 Mauro Giavalisco  <https://orcid.org/0000-0002-7831-8751>
 Christina C. Williams  <https://orcid.org/0000-0003-2919-7495>
 Henry C. Ferguson  <https://orcid.org/0000-0001-7113-2738>
 Yicheng Guo  <https://orcid.org/0000-0003-2775-2002>
 Teng Liu  <https://orcid.org/0000-0002-2941-6734>
 Bomee Lee  <https://orcid.org/0000-0003-1954-5046>

References

- Adelberger, K. L., Steidel, C. C., Pettini, M., et al. 2005, *ApJ*, 619, 697
 Baldry, I. K., Balogh, M. L., Bower, R. G., et al. 2006, *MNRAS*, 373, 469
 Baldry, I. K., Glazebrook, K., Brinkmann, J., et al. 2004, *ApJ*, 600, 681
 Balogh, M. L., Baldry, I. K., Nichol, R., et al. 2004, *ApJL*, 615, L101
 Bamford, S. P., Nichol, R. C., Baldry, I. K., et al. 2009, *MNRAS*, 393, 1324
 Barro, G., Faber, S. M., Koo, D. C., et al. 2015, *ApJ*, 840, 47
 Bertin, E., & Arnouts, S. 1996, *A&AS*, 117, 393
 Birrer, S., Lilly, S., Amara, A., Paranjape, A., & Refregier, A. 2014, *ApJ*, 793, 12
 Blanton, M. R., Eisenstein, D., Hogg, D. W., Schlegel, D. J., & Brinkmann, J. 2005, *ApJ*, 629, 143
 Blanton, M. R., & Moustakas, J. 2009, *ARA&A*, 47, 159
 Brammer, G. B., van Dokkum, P. G., & Coppi, P. 2008, *ApJ*, 686, 1503
 Bruzual, G., & Charlot, S. 2003, *MNRAS*, 344, 1000
 Cheung, E., Faber, S. M., Koo, D. C., et al. 2012, *ApJ*, 760, 131
 Coil, A. L., Mendez, A. J., Eisenstein, D. J., & Moustakas, J. 2017, *ApJ*, 838, 87
 Cooper, M. C., Newman, J. A., Coil, A. L., et al. 2007, *MNRAS*, 376, 1445
 Cucciati, O., Iovino, A., Marinoni, C., et al. 2006, *A&A*, 458, 39
 Dahlen, T., Mobasher, B., Faber, S. M., et al. 2013, *ApJ*, 775, 93
 Dekel, A., & Birboim, Y. 2006, *MNRAS*, 368, 2
 Drory, N., & Fisher, D. B. 2007, *ApJ*, 664, 640
 Fabian, A. C. 2012, *ARA&A*, 50, 455
 Farouki, R., & Shapiro, S. L. 1981, *ApJ*, 243, 32
 Fossati, M., Wilman, D. J., Mendel, J. T., et al. 2017, *ApJ*, 835, 153
 Franx, M., van Dokkum, P. G., Förster Schreiber, N. M., et al. 2008, *ApJ*, 688, 770
 Giavalisco, M., & Dickinson, M. 2001, *ApJ*, 550, 177
 Giavalisco, M., Ferguson, H. C., Koekemoer, A. M., et al. 2004, *ApJL*, 600, L93
 Giavalisco, M., Steidel, C. C., Adelberger, K. L., et al. 1998, *ApJ*, 503, 543
 Gómez, P. L., Nichol, R. C., Miller, C. J., et al. 2003, *ApJ*, 584, 210
 Grogin, N. A., Kocevski, D. D., Faber, S. M., et al. 2011, *ApJS*, 197, 35
 Gunn, J. E., & Gott, J. R., III 1972, *ApJ*, 176, 1
 Guo, Y., Bell, E. F., Lu, Y., et al. 2017, *ApJL*, 841, L22
 Guo, Y., Ferguson, H. C., Giavalisco, M., et al. 2013, *ApJS*, 207, 24
 Hamilton, A. J. S. 1993, *ApJ*, 417, 19
 Hatfield, P. W., & Jarvis, M. J. 2017, *MNRAS*, 472, 3570
 Hayashi, M., Shimasaku, K., Motohara, K., et al. 2007, *ApJ*, 660, 72
 Hogg, D. W., Blanton, M. R., Brinckmann, J., et al. 2004, *ApJL*, 601, L29
 Hopkins, P. F., Quataert, E., & Murray, N. 2012, *MNRAS*, 421, 3522

- Hsu, L.-T., Salvato, M., Nandra, K., et al. 2014, *ApJ*, 796, 60
- Kauffmann, G., White, S. D. M., Heckman, T. M., et al. 2004, *MNRAS*, 353, 713
- Kawinwanichakij, L., Papovich, C., Quadri, R. F., et al. 2017, *ApJ*, 847, 134
- Kawinwanichakij, L., Quadri, R. F., Papovich, C., et al. 2016, *ApJ*, 817, 9
- Koekemoer, A. M., Faber, S. M., Ferguson, H. C., et al. 2011, *ApJS*, 197, 36
- Kong, X., Daddi, E., Arimoto, N., et al. 2006, *ApJ*, 638, 72
- Landy, S. D., & Szalay, A. S. 1993, *ApJ*, 412, 64
- Larson, R. B., Tinsley, B. M., & Caldwell, C. N. 1980, *ApJ*, 237, 692
- Lee, B., Giavalisco, M., Whitaker, K., et al. 2018, *ApJ*, 853, 131
- Lee, K.-S., Giavalisco, M., Conroy, C., et al. 2009, *ApJ*, 695, 368
- Lee, K.-S., Giavalisco, M., Gnedin, O. Y., et al. 2006, *ApJ*, 642, 63
- Lin, L., Dickinson, M., Jian, H.-Y., et al. 2012, *ApJ*, 756, 71
- Mandelbaum, R., Seljak, U., Kauffmann, G., Hirata, C. M., & Brinkmann, J. 2006, *MNRAS*, 368, 715
- Martig, M., Bournaud, F., Teyssier, R., & Dekel, A. 2009, *ApJ*, 707, 250
- McGee, S. L., Bower, R. G., & Balogh, M. L. 2014, *MNRAS*, 442, L105
- Mobasher, B., Dahlen, T., Ferguson, H. C., et al. 2015, *ApJ*, 808, 101
- Mok, A., Balogh, M. L., McGee, S. L., et al. 2014, *MNRAS*, 438, 3070
- Moore, B., Lake, G., & Katz, N. 1998, *ApJ*, 495, 139
- Muzzin, A., Marchesini, D., Stefanon, M., et al. 2013, *ApJS*, 206, 8
- Muzzin, A., van der Burg, R. F. J., McGee, S. L., et al. 2014, *ApJ*, 796, 65
- Newman, A. B., Ellis, R. S., Andreon, S., et al. 2014, *ApJ*, 788, 51
- Papovich, C., Kawinwanichakij, L., Quadri, R. F., et al. 2018, *ApJ*, 854, 30
- Peebles, P. J. E. 1980, *The Large-scale Structure of the Universe* (Princeton, NJ: Princeton Univ. Press)
- Peng, Y., Maiolino, R., & Cochrane, R. 2015, *Natur*, 521, 192
- Peng, Y.-j., Lilly, S. J., Kovač, K., et al. 2010, *ApJ*, 721, 193
- Porciani, C., & Giavalisco, M. 2002, *ApJ*, 565, 24
- Santini, P., Ferguson, H. C., Fontana, A., et al. 2015, *ApJ*, 801, 97
- Schawinski, K., Urry, C. M., Simmons, B. D., et al. 2014, *MNRAS*, 440, 889
- Sobral, D., Best, P. N., Smail, I., et al. 2011, *MNRAS*, 411, 675
- Tinker, J. L., Robertson, B. E., Kravtsov, A. V., et al. 2010, *ApJ*, 724, 878
- Tomczak, A. R., Quadri, R. F., Tran, K.-V. H., et al. 2014, *ApJ*, 783, 85
- van den Bosch, F. C., Aquino, D., Yang, X., et al. 2008, *MNRAS*, 387, 79
- Wetzell, A. R., Tinker, J. L., Conroy, C., & van den Bosch, F. C. 2013, *MNRAS*, 432, 336
- Whitaker, K. E., Bezanson, R., van Dokkum, P. G., et al. 2017, *ApJ*, 838, 19
- Williams, R. J., Quadri, R. F., Franx, M., van Dokkum, P., & Labbé, I. 2009, *ApJ*, 691, 1879
- Wyder, T. K., Martin, D. C., Schiminovich, D., et al. 2007, *ApJS*, 173, 293